

# Fundamental Aspects of Alloy Plating

Prof. Dr. D. Landolt  
Recipient of  
AESF's 2000  
Scientific  
Achievement  
Award

**Electrodeposited alloys find many applications in the electronics, micromechanics and surface finishing industry. The composition of electroplated alloys is governed by the kinetics of the partial electrode reactions and it can be modeled in terms of mixed potential theory commonly used in corrosion science. Due to competitive adsorption phenomena at the electrode surface, the partial currents of codepositing metals can be larger or smaller than those in single metal plating under otherwise identical conditions. The present paper provides an overview of fundamental aspects of alloy deposition and of phenomena which determine deposit composition. The role of mass transport and current distribution is outlined, and modeling of anomalous and induced codeposition behavior is discussed and illustrated with examples. Pulse plating of alloys is considered taking into account the role of the displacement reactions during the off-time.**

Electrodeposited alloys find a wide range of applications in the electronics, metals and surface finishing industry and a large number of binary and ternary alloys have been plated from aqueous solutions for the purpose of microfabrication or surface coating.<sup>1,2</sup> Alloy plating permits to achieve tailor made properties for specific applications, but it requires closer control of deposition conditions than single metal plating. Increasing demands for improved functional performance (e.g., magnetism) and environmental pressures for replacement of certain metals (e.g., lead, chromium) are likely to further increase the importance of alloy plating in the future.

The functional properties of electrodeposited alloys depend on their chemical composition and on their structure on the micro and nano scales. Many factors affect the composition and microstructure of electrodeposited alloys; some of them are listed in Fig.1. In this paper, we shall focus on electrochemical phenomena which determine the alloy composition. For a discussion of structural aspects the reader is referred to the literature.<sup>3-5</sup>

Brenner, in his classic book on alloy deposition,<sup>1</sup> presented a comprehensive discussion of how electrochemical conditions affect the composition of electroplated alloys. Based mostly on thermodynamic arguments, he distinguished "normal" and "anormal" codeposition behavior. In "normal" codeposition, the more noble element deposits more readily and the composition of the deposit reflects that of the solution. "Anormal" behavior according to Brenner includes "anomalous" and "induced" codeposition. Anomalous codeposition means that the less noble metal deposits preferentially, as is typically observed during codeposition of the iron group metals Fe, Ni and Co with each other or with Zn. Induced codeposition indicates that a metal which can not be deposited in pure form can be codeposited as an alloy, well-known examples being the codeposition of molybdenum or tungsten with iron group metals. A more modern approach to codeposition, in addition to taking into account thermodynamics, must consider the kinetics of the partial electrode reactions as well as mass transport and homogeneous chemical reactions in the diffusion layer.<sup>6</sup> Using numerical modeling, codeposition reactions can be studied quantitatively in order to get a better understanding of how electrochemical mechanisms determine the composition of electrodeposited alloys.<sup>7</sup>

*Note: This is an edited version of Dr. Landolt's William Blum Lecture, delivered during SUR/FIN® 2001 in Nashville, Tennessee.*

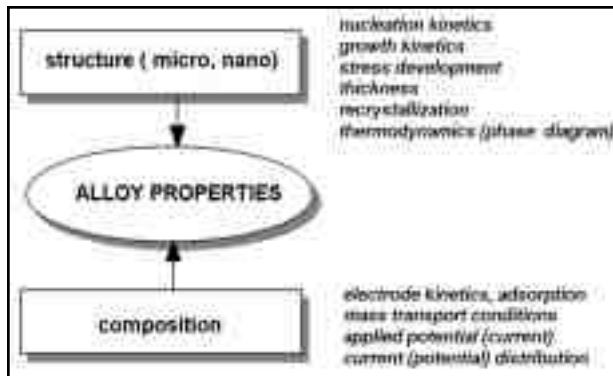


Fig. 1—Factors influencing the composition and structure of electroplated alloys.

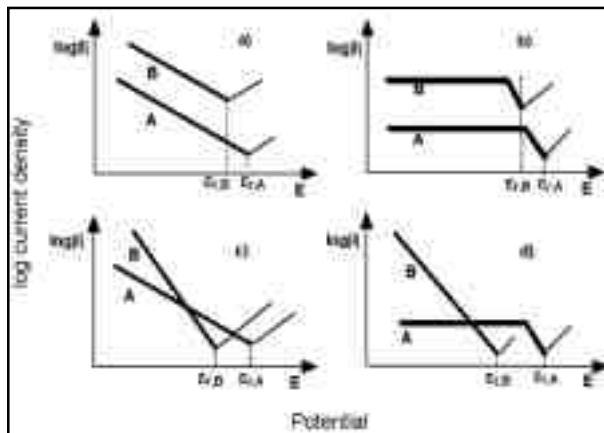


Fig. 2—Schematic showing the logarithm of the partial current densities for components A and B forming a binary alloy. Component A is thermodynamically more noble than B. (a): Both components are under activation control kinetics and exhibit identical Tafel slopes. (b): Both components exhibit a limiting current. (c): Both components deposit under activation control and exhibit different Tafel slopes. (d): Component A exhibits a limiting current, component B deposits under activation control.

The purpose of the present paper is to discuss fundamental aspects of alloy deposition and to show how the kinetics of partial reactions affect the resulting alloy composition. Experimental aspects related to the study of alloy deposition will be considered, and the importance of control of current distribution and mass transport conditions will be stressed. Theoretical models describing anomalous and induced codeposition will be briefly presented to illustrate the role of charge transfer kinetics, adsorption reactions and mass transport in alloy deposition. Finally, pulse plating of alloys will be discussed and the role of corrosion reactions taking place during the off-time and the effect of additives will be illustrated with examples.

### Basic Concepts

#### Mixed Electrodes

The theory of mixed electrodes was originally developed by Wagner and Traud<sup>8</sup> and later by Stern and Geary<sup>9</sup> to describe uniform corrosion. It states that the measured current density at

normally, during alloy deposition at least three electrochemical reactions proceed simultaneously on the cathode, the deposition of the alloy constituents and the formation of hydrogen. For deposition of a binary alloy AB this yields

$$i = i_A + i_B + i_H$$

where  $i_A$  and  $i_B$  are the partial current densities of alloy components A and B, respectively, and  $i_H$  is the current density for hydrogen formation. The current efficiency for alloy deposition and the composition of the deposited alloy can be expressed in terms of partial current densities. For deposition of a binary alloy AB, this yields for the current efficiency

$$\eta = \frac{i_A + i_B}{i}$$

and for the alloy composition (expressed as mole % of B)

$$X_B = \frac{i_B / n_B}{i_A / n_A + i_B / n_B} 100$$

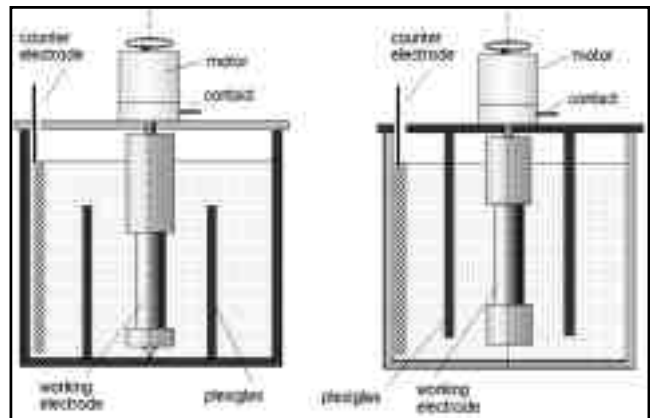


Fig. 3—Rotating Cylinder Hull (RCH) cell for electrodeposition studies. The current enters the cathode compartment either from the top or from the bottom.

a mixed electrode is the sum of the partial current densities of all anodic and cathodic reactions (anodic partial current densities are usually taken as positive and cathodic partial current densities as negative). At the corrosion potential (open circuit potential), the measured current density is zero and the sum of the anodic partial current densities is therefore equal to that of the cathodic partial current densities. Nor-

Here  $n_A$  is the charge number for the deposition of alloy component A, and  $n_B$  that for deposition of B. It follows from these equations that for given plating conditions the composition of electrodeposited alloys and the current efficiency are uniquely determined by the value of the partial current densities.

### Variation of Alloy Composition With Potential; Kinetic & Thermodynamic Aspects

Figure 2 illustrates how the kinetics of partial reactions affect the composition of electrodeposited alloys. It schematically shows plots of the logarithm of the partial current densities (absolute value) versus potential for different electrode kinetics typically encountered in alloy electrodeposition. One assumes deposition of a binary alloy AB, where A is the thermodynamically more noble element (equilibrium potential:  $E_{r,A} > E_{r,B}$ ). For simplicity the hydrogen reaction is not shown in the figure. Figure 2a presents a situation where both alloy elements codeposit under activation control, *i.e.*, the charge transfer at the electrode surface is rate limiting and the deposition obeys Tafel kinetics. The two Tafel slopes are assumed to be equal. At potentials more negative than  $E_{r,B}$  the ratio of the partial current densities for deposition of A and B is constant and therefore the composition of the deposited alloy is independent of potential. In Fig. 2b, both elements codeposit at the limiting current under diffusion control. Again, the alloy composition is constant over a wide potential range corresponding to the limiting current plateaus (in practice this situation might lead to dendrite formation, however). Figure 2c shows a situation where both elements codeposit under activation control, but con-

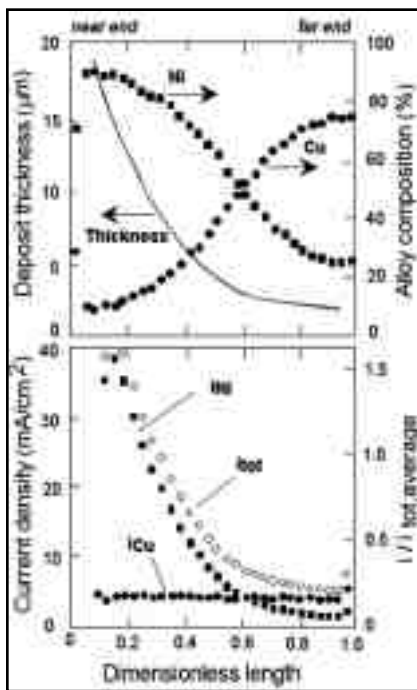


Fig. 4—Electrodeposition of Cu-Ni alloy using the RCH cell. The upper part of the figure shows the measured Cu and Ni content and the thickness of the deposit as a function of distance from the edge nearest to the anode. The lower part of the figure shows the partial current densities of Cu and Ni and the total current density derived from these data. The mass transport controlled partial current density of copper is uniform over the electrode, that of nickel decreases with increasing distance from the leading edge leading to a deposit rich in copper at the far end of the electrode (after ref. 18).

trary to Fig. 2a, the Tafel slope of element B here is higher than that of element A. The alloy composition therefore varies with potential. At not too cathodic potentials, the partial current density of A dominates and the deposited alloy contains mostly that element. On the other hand, at very negative potentials the partial current density of B dominates and the alloy deposit therefore contains mostly B. Note that over a wide potential range, the less noble element B deposits at a higher rate than the more noble element A. The thermodynamic equilibrium potential therefore gives no indication about the alloy composition resulting from codeposition. Figure 2d shows a situation where element A deposits under diffusion control and element B under activation control. At potentials positive to the equilibrium potential of B only the more noble element A deposits, while at very negative potentials deposition of B dominates. The described situation is typical for alloy plating electrolytes containing a noble element at low concentration and a less noble element at high concentration. Examples are cop-

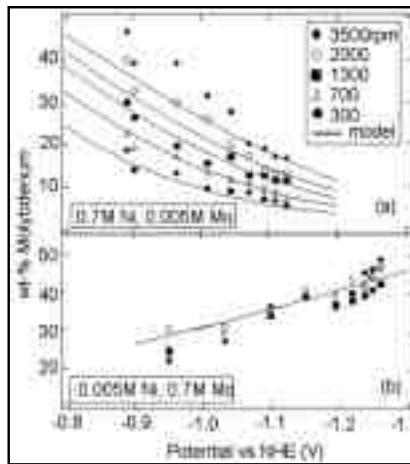


Fig. 5—Molybdenum content of Ni-Mo alloys measured on a rotating cylinder electrode at different rotation rates plotted as a function of applied potential. (a) Ni-rich electrolyte: 0.7M NiSO<sub>4</sub>, 0.005M Na<sub>2</sub>MoO<sub>4</sub>, 0.28M NH<sub>3</sub>, 0.7M Na-citrate; (b) Mo-rich electrolyte: 0.005M NiSO<sub>4</sub>, 0.7M Na<sub>2</sub>MoO<sub>4</sub>, 0.28M NH<sub>3</sub>, 0.005M Na-citrate (after ref. 30).

per-nickel and copper-cobalt electrolytes used for fabricating composition modulated multilayer alloys.<sup>10-13</sup>

Generally, the rate limiting step of a partial reaction depends on the concentration of the reacting species in the electrolyte and on their degree of complexing. Transport limited deposition is favored by a small concentration of the depositing species and absence of inhibition, while activation controlled deposition is favored by a high concentration and strong inhibition. Adsorption of codepositing species can also influence the partial reaction rates as will be discussed in a subsequent section.

## Experimental Considerations

### Determination of Partial Current Densities

To study the codeposition behavior one needs to know how the partial current densities vary with potential. Unfortunately, partial current densities can not be measured directly. Rather, their value must be calculated from the quantity and composition of the deposited alloy. For example, for a binary alloy AB and a deposit of thickness  $\Delta d$ , the partial current density of B is

$$i_B = \frac{n_B F}{M_B \Delta t} X_B^m \rho_{\text{alloy}} \Delta d$$

Here  $X_B$  is the mass fraction of element B in the alloy,  $M_B$  is the atomic mass of element B,  $\Delta t$  is the deposition-time,  $\rho_{\text{alloy}}$  is the density of the alloy and  $n_B$  is the charge number of element B. Note that  $\rho_{\text{alloy}} \Delta d$  corresponds to the total mass depos-

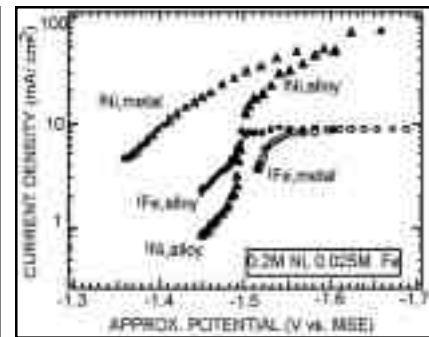


Fig. 6—Partial current densities of Ni and Fe for single metal and for alloy deposition in the RCH cell plotted vs. potential. The indicated potential scale was calculated from the primary current distribution. Electrolyte for alloy deposition: 0.2M NiSO<sub>4</sub>, 0.025M FeSO<sub>4</sub>, 0.4M H<sub>3</sub>BO<sub>3</sub>, 0.5M Na<sub>2</sub>SO<sub>4</sub>, pH 3. For single metal deposition, the equivalent amount of Na<sub>2</sub>SO<sub>4</sub> was added in replacement of NiSO<sub>4</sub> or FeSO<sub>4</sub> respectively (after ref. 22).

ited per surface area. One can therefore measure either the thickness or the mass of the deposit.

Different chemical and physical methods are available for determining the composition of deposited alloys. The average composition can be obtained by chemical solution analysis after chemical or electrochemical dissolution of the deposit or by physical methods such as X-ray fluorescence (XRF). Electron microprobe analysis, microspot XRF, or scanning Auger electron spectroscopy can be used to determine the local composition of alloy deposits.

### Control of Current Distribution & Mass Transport Conditions

In alloy deposition the uniformity of deposit thickness and composition depends on the partial current density distribution. Ideally, alloy deposition experiments therefore should be carried out under conditions of uniform partial current densities over the entire cathode. This requires a uniform potential distribution (primary current distribution) and uniform mass transport conditions, but in practice it is difficult to satisfy both requirements. In general, one therefore has to find a compromise between achieving a reasonably uniform primary current distribution and reasonably uniform mass transport conditions. In our laboratory, recessed rotating cylinder electrodes and recessed rotating disk or inverted rotating disk electrodes have been found particularly useful in that respect.<sup>14-16</sup>

A different approach often used in electroplating practice is based on the

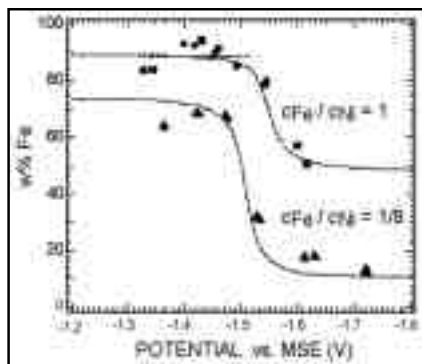


Fig. 7—Measured and calculated Fe content of Fe-Ni alloys deposited on a rotating cylinder electrode as a function of applied potential. Sulfate electrolytes (pH 3) containing 0.4M  $H_3BO_3$ . The Fe and Ni concentrations were varied between 0.025M and 0.2M to achieve different ratios of Fe/Ni in the solution (after ref. 36).

Hull cell.<sup>17</sup> The classic Hull cell has a highly non-uniform but well-characterized primary current distribution, permitting one to cover a wide range of current densities in a single experiment. On the other hand, mass transport conditions are not well controlled in the classical Hull cell. For this reason we developed the Rotating Cylinder Hull (RCH) cell.<sup>18,19</sup> It consists of a rotating cylinder electrode partially shielded by a tube made of an insulating material, usually plexiglas. The tube is open at one side, either at the top or at the bottom (Fig. 3). The current lines enter asymmetrically through the open end of the tube, yielding a highly non-uniform primary current distribution on the cathode. Through numerical optimization of the cell geometry the primary current distribution on the cathode can be made close to that of the classic Hull cell.<sup>18,20</sup> The mass transport conditions at the RCH cathode are those of a conventional rotating cylinder electrode, which means that the limiting current density is uniform and can be easily varied by varying the rotation rate.

Figure 4 illustrates the role of partial current distribution in alloy deposition. It shows results obtained with the RCH cell for the deposition of a Cu-Ni alloy from a sulfate-citrate electrolyte.<sup>18</sup> The average current density applied is 25 mA/cm<sup>2</sup>, the rotation rate 600 rpm. The upper part of the figure shows the deposit thickness and the Cu and Ni content (in mol%) of the alloy as a function of position along the cylinder electrode. These values were determined experimentally by microspot XRF. At the near end, with respect to the anode, the deposit thickness is highest. The nickel con-

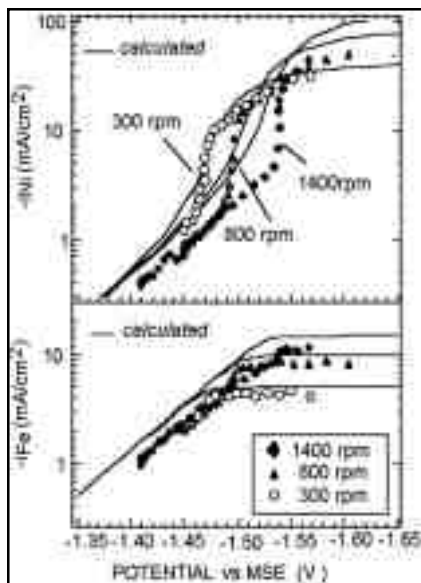


Fig. 8—Partial current densities of Ni and Fe measured with the RCH cell at different rotation rate during Ni-Fe deposition from a 0.5M  $Na_2SO_4 + 0.4M H_3BO_3$  electrolyte containing 0.025M  $FeSO_4$  and 0.2M  $NiSO_4$ . The lines represent calculated results. As the limiting current of Fe is reached the inhibition of nickel deposition ceases resulting in a strong increase in the Ni partial current density. (after refs. 22, 36).

tent decreases towards the far end, while the copper content increases. The lower part of the figure shows the partial current densities for Cu and Ni calculated from the analysis of the deposit. Also shown is the total current density representing the sum of the partial current densities of Cu and Ni (hydrogen evolution was negligible under the conditions of the experiment). The partial current density for nickel decreases strongly towards the far end of the electrode. Nickel is present in the electrolyte in high concentration and therefore deposits under activation control. Its partial current distribution reflects the non-uniform potential distribution. Copper is present in the solution at relatively low concentration, and under the conditions of the experiment it deposits under mass transport control. The copper partial current density therefore is uniform over the entire length of the cathode. Increasing the rotation rate increased the partial current density of Cu but did not significantly affect the partial current density of Ni.<sup>18</sup> The results shown illustrate well that in alloy plating one needs to control the potential distribution (primary current distribution), as well as the mass transport conditions at the cathode.

The RCH cell allows one to carry out alloy deposition experiments in which the current density (or the

potential) varies over a wide range, while maintaining uniform and reproducible mass transport conditions. In a single experiment a large variety of experimental conditions can thus be achieved. As a first approximation the overall current density as a function of position can be estimated from the published curves for primary current distribution.<sup>18</sup> If more accuracy is needed, the secondary or tertiary current distributions can be calculated by numerical simulation.<sup>21,22</sup> Generally, for a rapid evaluation of reaction conditions we prefer the approach based on primary current distribution, because it requires no numerical calculations.

### Enhancement & Inhibition of Partial Reactions by Codepositing Species Interactions Between Codepositing Species

To understand how the electrochemical conditions influence the composition of electrodeposited alloys one has to study the kinetics of the partial reactions. This includes the effect of mass transport processes and complexing equilibria on the concentration of reacting species at the cathode and the effect of competitive adsorption on the rate of charge transfer. The role of complexing equilibria in the electrodeposition of metals has been studied by Gerischer,<sup>23</sup> who showed that depending on concentration and applied potential, different complexed species react at the electrode. In alloy deposition the codepositing elements may compete for ligands and therefore the concentration of complexed species may differ from that observed in a comparable single metal electrolyte. The relative concentration of reacting species at the electrode surface is also affected by mass transport because they must be continuously replenished in the cathodic diffusion layer. Several groups<sup>24-27</sup> have presented mathematical models for alloy deposition, which included mass transport and complexing reactions. Local pH changes in the cathodic diffusion layer resulting from hydrogen evolution have been recently modeled also.<sup>28</sup> Competitive adsorption of codepositing species can affect the rate of charge transfer reactions and lead to acceleration or slowing down of the reaction rate of a given species compared to pure metal deposition. Typical examples of this behavior are anomalous codeposition of the iron group metals Fe, Ni and Co and induced codeposition of molybdenum.

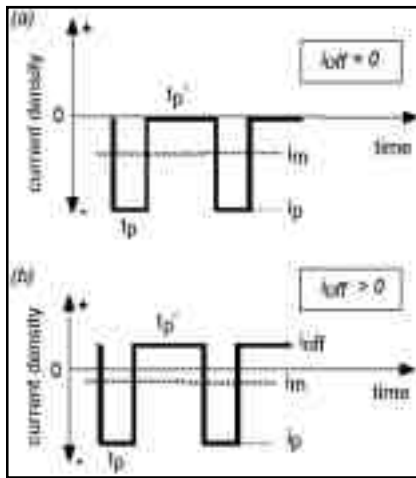


Fig. 9—Schematic of current density pulses. (a): the off-time current density is zero,  $i_{off} = 0$ ; (b): application of an anodic off-time current density,  $i_{off} > 0$ . The dotted line represents the average current density  $i_m$ . Also shown are the on-time  $t_p$ , the off-time  $t_p'$ , and the pulse current density  $i_p$ .

### Induced Codeposition of Mo with Ni

Induced codeposition of Mo and W is an example of enhancement of the rate of a partial reaction by a codepositing metal. It is well known that Mo can not be deposited from aqueous solution as a pure metal, but it readily codeposits with iron group elements forming alloys. In our laboratory we studied the mechanism of codeposition of Mo with Ni, Co and Fe.<sup>29,30</sup> To illustrate the coupling of Mo and Ni deposition, Fig. 5 shows the composition of Ni-Mo alloys electrodeposited from citrate electrolytes on a rotating cylinder electrode at different rotation rates. The electrolyte in Fig. 5a contained 0.7 M nickel and 0.005 M molybdate. The Mo content of the deposit increases with the rotation rate of the cylinder electrode. The reason is that due to the small concentration of molybdate in the solution the deposition of Mo is mostly controlled by mass transport. The electrolyte in Fig. 5b contained 0.005 M nickel and 0.7 M molybdate. In this case, the Mo content of the alloy varies with potential but is rather independent of rotation rate. Because Ni in this electrolyte is present at small concentration one would expect that it deposits under mass transport control while Mo, present in excess, should deposit under activation control. Such a mechanism would lead to a lower Mo content at higher rotation rate, contrary to the observed behavior. The fact that the alloy composition in Fig. 5b does not vary with rotation rate indicates that both metals deposit under mass transport control. In other words, the rate

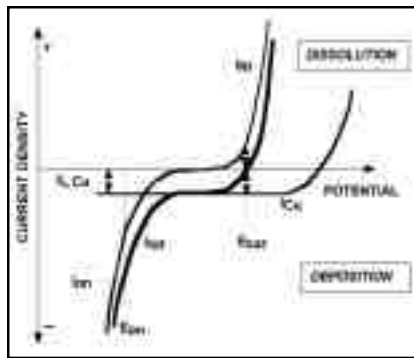


Fig. 10—Partial current densities of copper and nickel and total current density plotted as a function of potential (schematic). It is assumed that the Cu concentration in the electrolyte is much smaller than the Ni concentration. The corrosion potential  $E_{cor}$  corresponds to open circuit conditions where  $i_{tot} = 0$ . At this potential, Cu deposits at the limiting current density while Ni anodically dissolves. When a cathodic pulse current density is applied the Ni deposition is the dominating reaction.

of Mo deposition is limited by the rate of nickel deposition. The described behavior has been numerically modeled by Podlaha, *et al.*<sup>29</sup> The model used assumed that Mo deposition occurs through an adsorbed Ni-Mo reaction intermediate while Ni can deposit independently. In the electrolyte with low nickel concentration, the rate of Mo reduction therefore is governed by the transport of nickel to the electrode. In the electrolyte with low Mo concentration, however, nickel deposition occurs under activation control and mass transport of molybdate limits the reaction rate of Mo. The model thus explains the data of Fig. 5 as well as other results not shown here. In principle, a behavior as that shown in Fig. 5 could also result from reduction of a mixed Ni-Mo complex present in solution. However, spectroscopic studies have found no experimental evidence for the existence of Ni-Mo complexes for the electrolytes used.

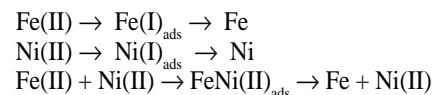
### Anomalous Codeposition of Iron Group Metals

Electrodeposition of Fe-Ni alloys has been studied extensively, because electrodeposited permalloy (81%Ni, 19%Fe) is widely used in the computer industry for the fabrication of magnetic heads.<sup>31</sup> This alloy exhibits anomalous behavior according to Brenner's classification, the Fe content in the deposit being much higher than expected from a consideration of the electrochemical behavior of the pure metals. Dahms and Croll,<sup>32</sup> in a classical paper, explained the anomalous

codeposition behavior by the presence of a hydroxide film on the cathode, which inhibits Ni deposition. However, more recent studies indicate that the behavior can be explained more readily by competitive adsorption of reaction intermediates.<sup>33,34</sup> According to this view, the adsorption of iron species at the cathode surface diminishes the surface area available for the reduction of Ni and thus leads to a reduction of the partial current density of this element.

Very recently, Zech, *et al.*,<sup>22,35,36</sup> Talbot and coworkers<sup>37,38</sup> observed that the codeposition of Fe not only has an inhibiting effect on Ni, but the codepositing Ni also enhances the rate of Fe deposition. Figure 6 illustrates this behavior. It shows the partial current densities of Ni and Fe measured in sulfate electrolytes during deposition of Ni-Fe alloy and of the pure metals, respectively. At a given potential the partial current density of Ni during alloy deposition is smaller than that observed for pure Ni deposition, while the partial current density of Fe is higher for alloy deposition than for pure metal deposition. At the potential where transport of Fe becomes rate limiting (about -1.5V MSE in Fig. 6) the enhancing effect disappears. The data of Fig. 6 demonstrate that the charge transfer reactions of the codepositing Fe and Ni are coupled.

To account for the described behavior, Zech, *et al.*<sup>36</sup> proposed a model where the inhibiting effect of Fe on codeposition of Ni is due to surface blocking and the accelerating effect of Ni on codeposition of Fe is due to formation of an adsorbed mixed reaction intermediate. The latter provides an additional reaction path for Fe reduction. The proposed enhancement mechanism is similar as that for induced codeposition of Mo. The electrode reactions according to the proposed model can schematically be written as follows:



Here Ni(II) and Fe(II) a divalent dissolved metal species, Ni(I)<sub>ads</sub> and Fe(I)<sub>ads</sub> are monovalent adsorbed reaction intermediates (hydrolyzed or not) and FeNi(II)<sub>ads</sub> is a mixed adsorbed reaction intermediate of intermediate valence (here two). The exact stoichiometry of the reaction intermediate is not known and is not critical for the

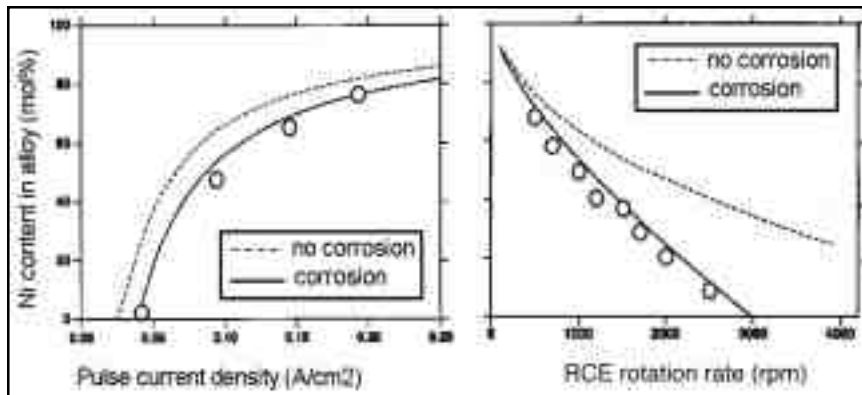


Fig. 11—Nickel content of pulse plated Ni-Cu alloys deposited on a rotating cylinder electrode from an electrolyte containing 0.7M NiSO<sub>4</sub>, 0.04M CuSO<sub>4</sub> and 0.26M Na-citrate. The effect of pulse current density at a constant rotation rate of 1000 rpm is shown as well as the effect of rotation rate at a constant pulse current density of -100mA/cm<sup>2</sup>. For all experiments:  $t_p = 4$  ms,  $t' = 16$  ms. The continuous line represents the prediction of the CM taking into account the off-time corrosion reaction, and the broken line represents the prediction of the NCM which assumes that no corrosion occurs during off-time (after ref. 38).

model predictions. Reduction of the mixed intermediate yields Fe and the original ionic species Ni(II). In presence of codepositing Ni, the Fe deposition therefore can follow two parallel reaction paths and its rate for given conditions can therefore exceed that of single metal deposition. On the other hand, the rate of reduction of Ni is diminished by the presence of the adsorbed reaction intermediates Fe(I)<sub>ads</sub> and FeNi(II)<sub>ads</sub> because they diminish the surface available for the nickel partial reaction. A detailed description of the model assumptions and of the equations used for the numerical simulation of the described behavior can be found in the original paper.<sup>36</sup>

To illustrate typical results obtained by numerical simulation, Fig. 7 shows calculated and measured Fe-Ni alloy compositions as a function of potential for two different ratios of Fe/Ni in the electrolyte (sulfate solutions, pH 3). All data were obtained at a rotating cylinder electrode at 800 rpm. At potentials up to about -1.5V the ratio of Fe/Ni in the deposit by far exceeds that in the electrolyte, a behavior typical for anomalous codeposition. At more cathodic potentials, however, the Fe/Ni ratio in the alloy is close to that in the solution. This can be explained by the fact that at high cathodic potentials Fe deposits under mass transport control at the limiting current. Under these conditions the charge transfer reaction is very rapid and the surface coverage of reaction intermediates of Fe is negligible. Nickel deposition therefore is no longer inhibited. Further support for the described mechanism comes from the observation that an increase in the rotation rate shifts

the transition from inhibited to non inhibited nickel deposition to higher potentials and higher current densities.<sup>22</sup>

Figure 8 shows the partial current densities of Fe and Ni measured in the RCH cell at different rotation rates.<sup>22</sup> The electrolyte contained 0.025 M FeSO<sub>4</sub> and 0.2M NiSO<sub>4</sub>. At high potentials Fe deposits at the limiting current while Ni deposition is activation controlled. The data of Fig. 8 show that as the limiting current density of Fe is reached the partial current density of nickel exhibits a jump because the Ni partial reaction is no longer inhibited by Fe codepositon. As the rotation rate is increased the limiting current of Fe increases and the jump in the nickel partial current density is shifted to higher currents. Also shown in Fig. 8 are calculated curves based on the model by Zech, *et al.*<sup>36</sup> Qualitatively the experimental behavior is well reproduced by the model, although the calculated values do not exactly match the experimental data. The difference may be due to uncertainties in the calculation of the potential in the RCH cell and to other limitations of the calculation. A similar behavior as for Fe-Ni alloys has been found for Fe-Co and Co-Ni alloys.<sup>35</sup> In all these alloy systems codeposition led to a decrease in the reaction rate of the more noble metal and to an enhancement of the reaction rate of the less noble metal.

### Codeposition Mechanisms

The above examples show that anomalous and induced codeposition can be understood and numerically modeled by considering the kinetics of the partial reactions and taking into

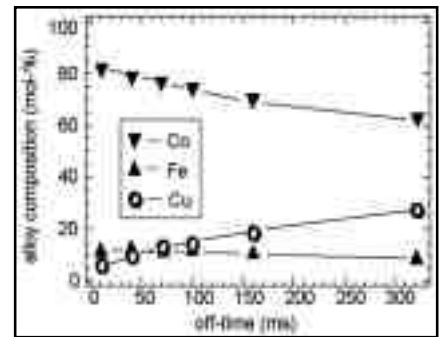


Fig. 12—Effect of off-time on the composition of pulse plated Co-Fe-Cu alloys. The solid lines represent the theoretical predictions of CM taking into account corrosion during off-time. Electrolyte: 0.3M CoSO<sub>4</sub>, 0.025M FeSO<sub>4</sub>, 0.025M CuSO<sub>4</sub>, 0.4M H<sub>3</sub>BO<sub>3</sub>, 0.1M Na-citrate, additives. Pulse plating parameters:  $t_p = 40$ ms,  $i_p = -220$  mA/cm<sup>2</sup>, 1000 rpm. (after ref. 43).

account possible interactions between the reacting species in solution and at the cathode surface. In a general way, three types of coupling of partial reactions can be distinguished in alloy deposition:<sup>6</sup>

- Non-interactive codeposition: The partial reaction rates of the codepositing species are independent of each other and therefore the alloy composition can be predicted from knowledge of the kinetics of the pure metals.
- Transport coupled codeposition: The partial reaction rates of the codepositing species are coupled through complexing equilibria and mass transport processes in the diffusion layer, which affect the surface concentration of reacting species.
- Charge transfer coupled codeposition: The partial reaction rates of the codepositing species are coupled through charge transfer kinetics, which involve adsorbed reaction intermediates. The latter can lead to a decrease (inhibition) or an enhancement of the reaction rate, typically found in anomalous and induced codeposition.

The three types of coupling behavior of partial reactions during codeposition provide a useful qualitative description of observed behavior. In practice, partial both solution equilibria and adsorption coupling of partial reactions may occur in the same system. A quantitative understanding of codeposition behavior can be achieved only through mathematical modeling. In the examples of induced and anomalous codeposition given above, the enhancement and

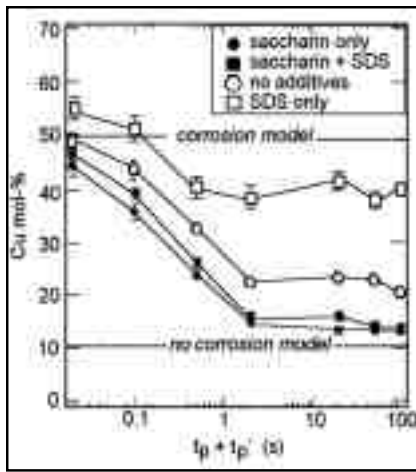


Fig. 13—Effect of additives on the composition of pulse plated Co-Cu alloys. The figure shows the mole fraction of Cu in the alloy as a function of pulse period for a constant duty cycle of 0.2. Pulse current density  $i_p = -40 \text{ mA/cm}^2$ , off-time current density  $i_{\text{off}} = 0.03 \text{ mA/cm}^2$ . Inverted rotating disk electrode at 1000 rpm. Electrolyte: 0.3M  $\text{CuSO}_4$ , 0.4M  $\text{H}_3\text{BO}_3$ , 0.1M Na-acetate, 0.005M  $\text{CuSO}_4$ , pH 4. Concentration of saccharin 2g/L and of SDS 0.2g/L. The broken lines indicate the theoretical prediction of the CM and NCM. (after ref. 46).

inhibition of partial reactions by codepositing species could be successfully modeled by postulating the presence of adsorbed reaction intermediates. It must be mentioned, however, that no independent proof for the existence of such species has been given so far. Other mechanisms leading to enhancement or inhibition of partial reaction rates should therefore not be excluded.

## Pulse Plating of Alloys

### Selection of Pulse Plating Parameters

The use of a pulsating current (pc) instead of a direct current offers additional possibilities to influence the composition and structure of alloy deposits. One generally distinguishes high frequency pulse currents, typically above 10 Hz, and low frequency pulse currents, typically well below 1 Hertz. When applying high frequency pulses, the amount of material deposited during one pulse cycle is so small that the deposit composition can be regarded as uniform throughout. In low frequency pulse plating, on the other hand, sufficient material is deposited during one pulse that the deposited alloy may exhibit a composition modulation due to different reactions taking place during the pulse on-time and the off-time. This behavior can be used to form layered structures, so called composition modulated (CMA) alloys,<sup>10,11</sup> which have found practical interest for magnetic applications. In the following, we shall dis-

cuss only high-frequency pulse plating of alloys and, in particular, we shall address the question of how the choice of electrical parameters affects alloy composition.

The simplest form of pulse plating uses current pulses followed by an off-time at open circuit (Fig. 9a), but for some applications a small cathodic or anodic off-time current may be applied (Fig. 9b). More complicated pulse sequences are possible, but shall not be considered here. An attractive feature of pulse plating is that the number of electrical variables that one can freely select is higher than in dc plating. Let us assume that we want to plate an alloy at a given average current density  $i_m$ . In pulse plating, assuming a zero off-time current,  $i_m$  depends on two variables, namely the applied pulse current density  $i_p$  and the duty cycle  $\theta$ .

$$i_m = i_p \theta \quad \text{with } \theta = t_p / (t_p + t_p')$$

Here  $t_p$  is the pulse-on-time and  $t_p'$  is the pulse-off-time. The non-steady state mass transport rate at the cathode depends on the absolute value of the these quantities. As a consequence, three variables,  $i_p$ ,  $\theta$  and  $t_p$  (or  $t_p'$ ) can be freely selected to achieve a given average current density. If a small cathodic or anodic current flows during the off-time, the average current density is

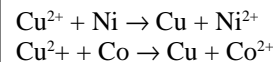
$$i_m = i_p \theta + i_{\text{off}} (1 - \theta)$$

where  $i_{\text{off}}$  is the off-time current density (anodic currents are taken as positive and cathodic currents as negative). Because  $i_{\text{off}}$  can be freely chosen, there are now four independent variables to be selected. With such a high number of variables, one needs theoretical models to guide experimental optimization of an alloy deposition process. To be practically useful, such models should be kept simple, however. The following examples involve such types of models.

### Pulse Plating Models for Cu-Ni & Cu-Co Alloys

In our laboratory, we developed theoretical models for the prediction of the composition of pulse plated binary alloys taking into account the reactions during the off-time. For these studies we used mainly Cu-Ni and Cu-Co alloys.<sup>16, 38-42</sup> Because Cu is thermodynamically much more noble than either Co or Ni, it deposits at less

cathodic potentials. In electrolytes of low Cu concentration and an excess of Ni or Co, the deposition of Cu takes place at the limiting current. For these conditions, theoretical models can be developed which take into account non-steady-state mass transport of Cu and activation controlled deposition of Co or Ni. Figure 10 illustrates schematically the described behavior. Over a wide potential range only Cu deposits, but at sufficiently cathodic potentials the partial current density of Ni or Co deposition is much higher than that for Cu. At the open circuit potential ( $i_{\text{off}} = 0$ ) a displacement reaction between the depositing Cu and the dissolving Ni or Co takes place:



To study the described behavior, Roy *et al.*<sup>38</sup> pulse plated Cu-Ni alloys from an electrolyte containing 0.26 M Na-citrate, 0.7M  $\text{NiSO}_4$ , 0.04M  $\text{CuSO}_4$  on a rotating cylinder electrode and compared the results with two models describing limiting behavior. In the "corrosion model" (CM) it was assumed that Cu continues to deposit under limiting current conditions during the off-time leading to a corresponding amount of Ni dissolution. In the second model, the "no-corrosion model" (NCM), it was assumed that no displacement reaction takes place during the off-time. Figure 11 shows the measured nickel content of the pulse-plated Ni-Cu alloy for different pulse current densities and different rotation rates using a constant pulse off-time of 16 ms. Also shown are calculated curves for the CM and the NCM. Good agreement with the CM is observed for the conditions of the experiments.

Due to the short pulse off-time, the amount of copper deposited by the displacement reaction during  $t_{\text{off}}$  is sufficiently small so as not to significantly block the cathode surface. However, at larger pulse off-times increasing amounts of Cu deposit and a thin copper layer may build up at the electrode surface during  $t_{\text{off}}$ . The copper deposit acts as a screen, and increasingly slows down the rate of the displacement reaction. In the limiting case, when a compact Cu layer covers the entire electrode surface the displacement reaction will cease altogether. The alloy composition should then approach that predicted by NCM. At intermediate off-times the Cu content of the pulse plated alloys is

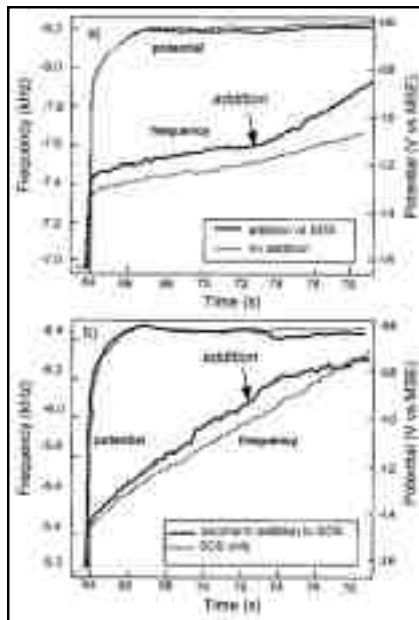


Fig. 14—Effect of additive addition on the rate of the displacement reaction during the off-time during pulse plating of a Cu-Co alloy. The frequency change measured with the rotating quartz crystal microbalance (rEQCM) is a measure for the mass change of the electrode. (a): Upon addition of SDS the slope of the frequency versus time curve increases indicating a higher corrosion rate. (b): Upon addition of saccharin to an SDS containing electrolyte the slope of the frequency versus time curve decreases indicating a decrease in corrosion rate. Also shown in the figure are the measured potentials which change only little upon addition of additives. Pulse period 20s, duty cycle 0.2, sulfate electrolyte, pH 4. (after ref. 46).

expected to vary with the off-time (or duty cycle) between the value predicted by the CM and the value predicted by the NCM.<sup>38</sup> Mathematical modeling of the limiting cases of CM and NCM is relatively easy, but modeling of the intermediate situation is difficult, because the effect of the deposited copper on the rate of the displacement reaction must be taken into account. The importance of it depends on the porosity of the deposit and on its morphology, and is not readily expressed in terms of mathematical equations. To avoid dealing with these problems, a simple approximation has been proposed assuming that during the off-time a non-covered part of the surface corrodes according to CM, while the remainder of the surface is protected by a Cu film and does not corrode.<sup>41</sup> Experimental data for Cu-Co alloys could be interpreted in a rational way based on this concept.<sup>42</sup>

### Predicting Composition of Ternary Alloys

In special situations, the CM and NCM models developed for pulse plat-

ing of binary alloys can be applied to ternary alloys, namely when two of the three alloy components are present in the electrolyte at low concentration and deposit under mass transport control. In our laboratory, we recently studied pulse plating of Co-Fe-Cu alloys from an electrolyte containing small concentrations of Cu and Fe and a large concentration of Co.<sup>43</sup> From such a solution, Cu and Fe deposit under mass transport control and Co under activation control. During the off-time the more noble Cu undergoes a displacement reaction with Fe and Co. One would therefore expect that an increasing off-time leads to a higher Cu concentration in the alloy. On the other hand, because iron does not displace cobalt the Fe/Co ratio should be largely independent on off-time. Furthermore, because Fe deposits under non-steady-state diffusion conditions the ratio Fe/Co in the alloy should decrease with increasing on-time. Based on these considerations, it should be possible to vary the relative concentration of the three alloy elements by simply changing the pulse parameters, keeping the average current density, hydrodynamic conditions, and electrolyte composition the same. The results of Fig. 12, showing experiments in which the off-time was varied, confirm this behavior.<sup>43</sup> It is interesting to note that pulse plating permits to achieve ternary alloy compositions that can not readily be obtained by dc plating from the same electrolyte. For example, under the experimental conditions of Fig. 12 deposition of Fe and Cu is mass transport controlled. In dc plating, for a given electrolyte composition, the concentration of the two elements in the alloy could be varied by changing the hydrodynamic conditions. However, their concentration in the alloy would evolve in parallel, because both limiting currents vary the same way with convection conditions. In pulse plating, on the other hand, the concentration of Cu in the alloy, contrary to that of Fe, increases with increasing off-time due to the displacement reaction. By varying the off-time, one therefore can selectively vary the copper content of the alloy without a corresponding change in Fe content.

### Additive Effects

Most practical plating electrolytes contain additives such as leveling agents, stress relievers, brighteners, surfactants, etc. In alloy plating, additives or combinations of additives can

affect the composition of the electrodeposits. Figure 13 illustrates this effect for pulse plated Co-Cu alloys.<sup>44</sup> The alloy was plated from a sulfate-acetate electrolyte (pH 4) on an inverted rotating disk electrode at 1000 rpm using a pulse current density of 40 mA/cm<sup>2</sup> and a constant duty cycle of 20 percent. The pulse period was varied. Plating experiments were carried out in presence and absence of the additives SDS, which is a surfactant, and saccharin, which is a stress-relieving agent. All results show a decrease of copper content with increasing pulse period, as one may expect from a consideration of the CM and NCM discussed in the previous paragraph. The model predictions are shown in Fig. 13 by the broken lines. With increasing pulse period (at constant duty cycle) the pulse off-time becomes longer. As a consequence, the rate of the displacement reaction diminishes and the behavior approaches that predicted by NCM. The data of Fig. 13 show that the additives have a major effect on the described behavior and therefore on the copper content of the alloy. Adding saccharin alone or in combination with SDS leads to a slightly lower copper content at long pulse periods compared to plating without additives, but the effect is relatively small. Surprisingly, adding only SDS leads to a much higher copper content at long off-times. Apparently, SDS enhances the rate of the displacement reaction at long pulse off-times, but the presence of saccharin eliminates this effect.

To get more information on the observed behavior, Kelly *et al.*<sup>45</sup> performed a series of experiments with a rotating electrochemical quartz crystal microbalance (rEQCM). The electrochemical quartz crystal microbalance measures the change in resonance frequency of a quartz crystal coated with a thin metal film used as a working electrode in an electrochemical cell. According to the well-known Sauerbrey equation, the frequency shift is directly proportional to the mass change resulting from deposition or dissolution. The high mass sensitivity of the electrochemical quartz crystal microbalance, on the order of fractions of a monolayer, permits one to monitor tiny mass changes that occur during the pulse off-time. In pulse plating of Cu-Co alloys, the displacement reaction between copper and cobalt during pulse off-time results in a slight mass gain of the electrode because the atomic mass of Cu

(63.5g/mol) is slightly higher than that of Co (58.9 g/mol). In Fig. 14a, the measured frequency change during the off-time of a given pulse cycle is shown for two conditions, an experiment in the absence of additive and an experiment involving with addition of SDS during the off-time.<sup>46</sup> As SDS is added (arrow), the slope of the frequency-time curve becomes steeper indicating a larger mass gain. Also shown in the figure is the potential, which does not significantly change. The results confirm that SDS enhances the rate of the displacement reaction. Further experiments not shown here indicated that SDS is consumed in the process and that its reaction rate is at least partly controlled by mass transport. A similar experiment was performed by adding saccharin during the off-time to an electrolyte containing SDS (Fig. 14b). The results show that addition of saccharin leads to a decrease of the slope of the frequency-versus-time curve, indicating a decrease in the rate of the displacement reaction. This confirms that saccharin neutralizes the accelerating effect of SDS on the displacement reaction in agreement with the results of Fig. 13. The described results suggest that in presence of only SDS, the copper deposited during the off-time is less compact than that deposited in presence of both additives. The detailed mechanism by which the two additives interact at the surface and influence the deposition process is not known currently and needs further study.

### Concluding Remarks

The scientific understanding of alloy deposition and how the kinetics of electrochemical reactions affect the composition of electrodeposits has significantly advanced in recent years. The role of mass transport, current distribution and charge transfer kinetics has been identified, and a number of alloy deposition systems have been successfully modeled using mixed potential theory and considering interactions between codepositing species. It has been found that coupling of charge transfer reactions through adsorbed reaction intermediates can decrease or enhance the rate of partial reactions, thereby providing a rational explanation of anomalous and induced codeposition. Pulse plating enlarges the choice of free variables and can lead to alloy compositions not readily achieved with dc plating under com-

parable conditions. For certain binary and ternary alloy systems, theoretical models that take into account the role of the displacement reaction during off-time permit one to predict the effect of applied pulse parameters on alloy composition.

At present, the primary usefulness of theoretical models for alloy deposition lies in their capability to rationalize observed behavior and to predict the effect of certain variables. Modeling can therefore serve as a guide for the optimization of deposition conditions. Only a limited number of alloy systems have been theoretically modeled so far, however, and there is room for improvement of the models. In particular, there is a need for models that predict codeposition behavior of charge transfer-coupled reactions from experiments with pure metals; at present the rate constants needed must be measured on alloys. The role of complexing equilibria and pH changes near the cathode surface needs further study. The availability of user-friendly software based on realistic physical assumptions could greatly help to simulate practical alloy plating problems without the need for extensive programming. There is also a need for a better understanding of synergistic and antagonistic effects of additives on a microscopic level, and how these affect the composition and structure of alloy deposits. Quantitative models that describe the development of the micro- and nanostructure of electrodeposited alloys under realistic conditions are mostly lacking at present. Obviously, there is a strong need for more research in the field of alloy deposition.

### Acknowledgement

The results shown in this paper are the work of many persons who were members of our laboratory at one time or another (in alphabetical order): P. Bradley, J. Kelly, P. Kern, C. Madore, M. Matlosz, E.J. Podlaha, S. Roy, A. West, N. Zech. The author thanks A. Marlot for critically reading the manuscript. For many years, Fonds National Suisse, Bern, has provided financial support for our research on electrodeposition and dissolution. *P&SF*

### References

1. A. Brenner, *Electrodeposition of Alloys*, Vol. I & II, Academic Press New York (1963).
2. M. Schlesinger, M. Paunovic, *Modern Electroplating*, 4th Edition, J. Wiley New York (2000).

3. R. Winand, *Electrochim. Acta*, **39**, 1091 (1994).
4. E. Budevski, G. Staikow, W.J. Lorenz, *Electrochemical Phase Formation & Growth*, VCH Weinheim (1996), 410.
5. D. Landolt, *Electrochemically Deposited Thin Films III*, M. Paunovic, D. Shearson, Eds., Electrochem. Soc. Inc., Pennington N.J. (1997) p. 160.
6. D. Landolt, *Electrochim. Acta*, **39**, 1075 (1994).
7. D. Landolt, E.J. Podlaha, N. Zech, *Z. Phys. Chem.* **208**, 167 (1999).
8. C. Wagner, W. Traud, *Z. Elektrochem.*, **44**, 391 (1938).
9. M. Stern & A. L. Geary, *J. Electrochem. Soc.* **104**, 56 (1957).
10. J. Yahalom & O. Zadok, *J. Mater. Sci.*, **22**, 499 (1987).
11. D.S. Lashmore & M.P. Dariel, *J. Electrochem. Soc.*, **135**, 1218 (1988).
12. C. Bonhôte, D. Landolt, *Electrochim. Acta.*, **42**, 2407 (1997).
13. J.J. Kelly, P. Bradley, D. Landolt, *J. Electrochem. Soc.*, **147**, 2975 (2000).
14. T.E. Dinan, M. Matlosz, D. Landolt, *J. Electrochem. Soc.*, **138**, 2947 (1991).
15. P. Bradley, D. Landolt 144, L145 (1997).
16. P.E. Bradley, D. Landolt, *Electrochim. Acta.*, **45**, 1077 (1999).
17. R.O. Hull, *Trans. Am. Electroplat. Soc.*, **27**, 52 (1939).
18. C. Madore, D. Landolt, *Plating & Surf. Finish.*, **80**(11), 73 (1993).
19. C. Madore, D. Landolt, C. Hassenpflug, J.A. Hermann, *Plating Surf. Finish.*, **82**(8), 36 (1995).
20. C. Madore, A.C. West, M. Matlosz, D. Landolt, *Electrochim. Acta.*, **37**, 69 (1992).
21. C. Madore, M. Matlosz, D. Landolt, *J. Appl. Electrochem.*, **22**, 1155 (1992).
22. N. Zech, E.J. Podlaha, D. Landolt, *J. Appl. Electrochem.*, **28**, 1251 (1998).
23. H. Gerischer, *Chem. Ing. Techn.*, **36** (6), 666 (1964).
24. A. Survila, Z. Mockus, S. Kanapeckaite, *Electrochim. Acta.*, **46**, 571 (2000).
25. R.Y. Ying, P. K. Ng, Z. Mao, R.E. White, *J. Electrochem. Soc.*, **135**, 2964 (1988).
26. M.F. Mathias, T.W. Chapman, *J. Electrochem. Soc.*, **137**, 102 (1990)
27. E.J. Podlaha, C. Bonhôte, D.

- Landolt, *Electrochim. Acta.*, **39**, 2649 (1994).
28. N. Zech, D. Landolt, *Electrochim. Acta.*, **45**, 3461 (2000).
29. E.J. Podlaha, D. Landolt, *J. Electrochem. Soc.*, **143**, 885 (1996).
30. E.J. Podlaha, D. Landolt, *J. Electrochem. Soc.*, **143**, 893 (1996).
31. P.C. Andricacos, L.T. Romankiw, *Advances in Electrochemical Science & Engineering*, Vol. 3, H. Gerischer, C.W. Tobias Eds., VCH Weinheim (1994), p. 227.
32. H. Dahms, I.M. Croll, *J. Electrochem. Soc.*, **112**, 771 (1965).
33. M. Matlosz, *J. Electrochem. Soc.*, **140**, 2272 (1993).
34. S. Hessami, C. W. Tobias, *J. Electrochem. Soc.*, **136**, 3611 (1989).
35. N. Zech, E.J. Podlaha, D. Landolt, *J. Electrochem. Soc.*, **146**, 2886 (1999).
36. N. Zech, E.J. Podlaha, D. Landolt, *J. Electrochem. Soc.*, **146**, 2892 (1999).
37. K.S. Sasaki, J.B. Talbot, *J. Electrochem. Soc.*, **145**, 981 (1998).
38. K.Y. Sasaki, J. B. Talbot, *J. Electrochem. Soc.*, **147**, 189 (2000).
38. S. Roy, M. Matlosz, D. Landolt, *J. Electrochem. Soc.*, **141**, 1509 (1994).
39. S. Roy, D. Landolt, *J. Electrochem. Soc.*, **142**, 3021 (1995).
40. P. Bradley, S. Roy, D. Landolt, *J. Chem. Soc. Farad. Trans.*, **92**, 4015 (1996).
41. P. Bradley, D. Landolt, *Electrochim. Acta.*, **42**, 993 (1997).
42. P. E. Bradley, D. Landolt, *Electrochim. Acta.*, **45**, 1077 (1999).
43. P. Bradley, B. Janossy, D. Landolt, *J. Appl. Electrochem.*, **31**, 137 (2001).
44. J.J. Kelly, P. Bradley, D. Landolt, *J. Electrochem. Soc.*, **147**, 2975 (2000).
45. P. Kern, D. Landolt, *J. Electrochem. Soc.*, **147**, 318 (2000).
46. J.J. Kelly, P. Kern, D. Landolt, *J. Electrochem. Soc.*, **147**, 3725 (2000).

#### About the Author

*Professor Dr. Dieter Landolt is a professor of materials science and head of the Laboratory of Metallurgical Chemistry, Swiss Federal Institute*



*of Technology Lausanne (EPFL), Switzerland. His research focuses on the fundamental aspects of electrochemical surface treatment and microfabrication processes;*

*alloy deposition, modeling and cell design; corrosion and protection of metals; passivity; surface analysis by AES, EXP and SIMS; and chemical effects in tribology and tribocorrosion.*

*He is author or co-author of more than 230 publications in refereed journals and conference proceedings, and author of a textbook on surface chemistry and corrosion of metals. A longtime member of AESF's International Branch, he is considered to be the leading academic in the field of surface finishing in Switzerland. He leads an internationally respected research group and is a frequent speaker at conferences worldwide. He was the recipient of AESF's 2000 Scientific Achievement Award.*